Whole-Body Tumor Imaging Using PET and 2-^{18}F-Fluoro-L-Tyrosine: Preliminary Evaluation and Comparison with ^{18}F-FDG

Roland Hustinx, MD, PhD[1]; Christian Lemaire, PhD[2]; Guy Jerusalem, MD[3]; Pierre Moreau, MD[4]; Didier Cataldo, MD[5]; Bernard Duysinx, MD[5]; Joel Aerts, MS[2]; Marie-France Fassotte, MD[3]; Jacqueline Foidart, MD[1]; and André Luxen, PhD[2]

[1]Division of Nuclear Medicine, University Hospital, Liège, Belgium; [2]Cyclotron Research Center, University of Liège, Liège, Belgium; [3]Division of Hematology-Oncology, University Hospital, Liège, Belgium; [4]Department of Otolaryngology, University Hospital, Liège, Belgium; and [5]Division of Pulmonary Medicine, University Hospital, Liège, Belgium

^{18}F-FDG PET imaging is now established as a valuable tool for evaluating cancer patients. However, a limitation of ^{18}F-FDG is its absence of specificity for tumor. Both protein synthesis and amino acid transport are enhanced in most tumor cells, but their metabolism is less affected in inflammation. We therefore decided to evaluate the ability of PET with 2-^{18}F-fluoro-L-tyrosine (^{18}F-TYR) to visualize cancer lesions in patients compared with ^{18}F-FDG PET. **Methods:** ^{18}F-FDG PET and ^{18}F-TYR PET were performed on 23 patients with histologically proven malignancies (11 non–small cell lung cancers (NSCLCs), 10 lymphomas, and 2 head and neck carcinomas). Fully corrected, whole-body PET studies were obtained on separate days. ^{18}F-FDG studies were performed after routine clinical fashion. ^{18}F-TYR studies were started 36 ± 6 min after tracer injection and a second scan centered over a reference lesion was acquired after completion of the whole-body survey—on average, 87 min after injection. Standardized uptake values (SUVs) were calculated for all abnormal foci and for various normal structures. Results were compared with pathologic or correlative studies. **Results:** ^{18}F-FDG PET correctly identified 54 malignant lesions, among which 36 were also visualized with ^{18}F-TYR (67%). ^{18}F-TYR did not detect any additional lesion. Tumor SUVs (SUV_{bw}, 5.2 vs. 2.5), tumor-to-muscle (7.4 vs. 2.7), and tumor-to-mediastinum activity ratios (3 vs. 1.4) were higher with ^{18}F-FDG than with ^{18}F-TYR. Two of 11 NSCLCs and 4 of 10 lymphomas were understaged with ^{18}F-TYR compared with ^{18}F-FDG. Although the NSCLC lesions missed by ^{18}F-TYR PET were small, several large lymphoma lesions did not accumulate the tracer. In 4 patients, ^{18}F-TYR–positive lesions coexisted with ^{18}F-TYR–negative lesions. There was a high physiologic ^{18}F-TYR uptake by the pancreas (average SUV_{bw}, 10.3) and the liver (average SUV_{bw}, 6.3). Muscle and bone marrow uptakes were also higher with ^{18}F-TYR than with ^{18}F-FDG: average SUV_{bw}, 1 versus 0.7 and 2.6 versus 1.8, respectively. There was no change over time in the ^{18}F-TYR uptake by the tumors or the normal structures. **Conclusion:** ^{18}F-TYR PET is not superior to ^{18}F-FDG PET for staging patients with NSCLC and lymphomas.

Received Jul. 15, 2002; revision accepted Oct. 24, 2002.
For correspondence or reprints contact: Roland Hustinx, MD, PhD, Service de Médecine Nucléaire, CHU du Sart Tilman, B35, 4000 Liège 1, Belgium.
E-mail: rhustinx@chu.ulg.ac.be

Key Words: 2-^{18}F-fluoro-L-tyrosine; ^{18}F-FDG; PET; cancer; protein synthesis

J Nucl Med 2003; 44:533–539

During the past decade, PET imaging has become an essential tool in the management of a growing number of cancer patients (*1*). ^{18}F-FDG is by far the most common radiopharmaceutical in clinical use and has shown a high sensitivity for diagnosing and staging a wide variety of malignant diseases. However, there are several well-known limitations for the use of ^{18}F-FDG in oncology. Glucose metabolism is not significantly increased in some tumor types, such as prostate carcinoma (*2*). The most significant drawback of ^{18}F-FDG for oncologic purposes results from its absence of specificity for tumor. Infection, inflammation, granulomatous diseases, and many other physiologic or pathologic conditions can all show high ^{18}F-FDG uptake (*3*).

Protein metabolism is also highly modified in tumor cells. Both amino acid transport and protein synthesis rate are enhanced in malignancies (*4*,*5*). In contrast to ^{18}F-FDG, amino acids appear to play a marginal role in the metabolism of inflammatory cells (*6*). Radiolabeled amino acids may thus be more suited than ^{18}F-FDG for tumor imaging (*7*). Although the majority of the amino acids that were proposed as radiopharmaceuticals for evaluating protein metabolism with PET were labeled with ^{11}C (*7*), ^{18}F has a longer physical half-life, which improves its availability and potential for clinical use.

The synthesis of 2-^{18}F-fluoro-L-tyrosine (^{18}F-TYR) was first reported in 1988, and initial studies showed the potential of the tracer for evaluating protein synthesis in brain tumors (*8*,*9*). Recently, Lemaire et al. (*10*) modified the synthesis so that the tracer can now be produced as a no–carrier-added compound, with high yields and high specific activity. We therefore decided to conduct the first

clinical investigation of ^{18}F-TYR as a tracer for whole-body tumor imaging.

MATERIALS AND METHODS

Radiopharmaceutical Preparation and Purity

No–carrier-added ^{18}F-TYR was produced via a multistep procedure (*10*). The first part of the synthesis involves the nucleophilic substitution of a 2-trimethylammonium-4-methoxy-benzaldehyde triflate with ^{18}F-fluoride produced by the ^{18}O(p,n) nuclear reaction. The ^{18}F-fluorobenzaldehyde derivative was trapped on a solid support and then converted into the corresponding ^{18}F-fluorobenzyl bromide by treatment with $NaBH_4$ and HBr. The last steps of the synthesis imply alkylation of a (diphenylmethylene)-glycine tert-butyl ester compound by phase-transfer catalysis with a C_2-symmetric chiral catalyst (*11*), acid hydrolysis and high-performance liquid chromatography purification. ^{18}F-TYR was then obtained with a radiochemical yield of 25%–40% (decay corrected, 100 min). This procedure affords at the end of the synthesis 4.9−7.8 GBq ^{18}F-TYR of high specific activity.

Enantiomeric purity was determined on a CrownPak CR(+) column (Daicel, Tokyo, Japan) eluted at a flow rate of 0.8 mL/min with $HClO_4$ (pH 4). In all cases, enantiomeric purity and radiochemical purity were >95% and >99%, respectively. Other quality controls (pH, osmolality, γ-purity, solvent, and so forth) were also realized.

^{18}F-FDG was synthesized according to Lemaire et al. (*12*) using an automated ^{18}F-FDG synthesis system (Coincidence Technologies S.A., Liège, Belgium).

Patients

Twenty-three patients (15 men, 8 women; mean age, 67 ± 8 y) were enrolled in this prospective study. All subjects had a pathologically proven malignancy. There were 11 non–small cell lung cancers (NSCLCs), 10 lymphomas, and 2 head and neck carcinomas. In all but 1 case, PET scanning was performed before any treatment was initiated. One patient with an intermediate-grade non-Hodgkin's lymphoma (NHL) received chemotherapy (etoposide-dexamethasone) 6 wk before the PET. At that time, she was being reevaluated because of an apparent lack of response to this treatment. The patients' characteristics are listed in Table 1. The medical ethics committee of our institution approved the research protocol, and all patients gave a written informed consent.

PET

All studies were performed using the C-PET scanner (UGM-Philips, Milpitas, CA). The system has been fully described elsewhere (*13*). ^{18}F-FDG and ^{18}F-TYR PET studies were performed within 1 wk of each other. All patients fasted for at least 4 h before tracer injection. The blood glucose level was measured in each case and did not exceed 7.7 mmol/L. Patients with lymphoma received Diazepam (Valium; Roche S.A., Brussels, Belgium), 5 mg orally, 15 min before injection of ^{18}F-FDG to limit muscle

TABLE 1
Patient Characteristics

Patient no.	Age (y)	Sex	Primary	Pathology	Confirmation	Clinical stage	^{18}F-FDG stage	^{18}F-TYR stage
1	75	M	Lung	SCC	Biopsy	T4 N1 M0	T+ N1 M0	T+ N1 M0
2	77	F	Lymphoma	LG NHL	Surgery	I	I	I
3	72	M	Lung	SCC	Surgery	T2 N0 M0	T+ N0 M0	T+ N0 M0
4	83	F	Lung	LCC	Biopsy	T4 N1 Mx	T+ N1 M1	T+ N1 M0
5	52	M	Tongue	SCC	Biopsy	T4 N2 M0	T+ N2 M0	T+ N2 M0
6	77	M	Lung	SCC	Biopsy	T1 N1 M0	T+ N1 M0	T+ N1 M0
7	68	F	Lymphoma	HD	Biopsy	IV	IV	II
8	67	M	Lung	SCC	Biopsy	T4 N0 M0	T+ N0 M0	T+ N0 M0
9	65	F	Lymphoma	IG NHL	Biopsy	IV	II	II
10	69	F	Tonsil	SCC	Surgery	T2 N0 M0	T+ N0 M0	T+ N0 M0
11	67	M	Lung	LCC	Surgery	T2 N0 M0	T+ N1 M0	T+ N0 M0
12	63	M	Lung	Adenoc.	Surgery	T2 N2 M0	T+ N2 M0	T+ N0 M0
13	56	M	Lymphoma	LG NHL	Biopsy	IIIA	III	III
14	72	M	Lymphoma	HG NHL	Biopsy	IV	IV	II
15	74	M	Lymphoma	IG NHL	Biopsy	III	III	III (−)
16	69	M	Lung	SCC	Biopsy	T2 N0 M0	T+ N0 M0	T+ N0 M0
17	54	M	Lung	Adenoc.	Surgery	T1 N0 M0	T+ N0 M0	T+ N0 M0
18	71	F	Lymphoma	LG NHL	Biopsy	IA	FN	FN
19*	52	F	Lung	SCC	Surgery	T1 N0 M1	T+ N0 M0	FN
20	59	M	Lung	Adenoc.	Surgery	T1 N0 M0	T+ N1 M0	T+ N0 M0
21	64	F	Lymphoma	LG NHL	Biopsy	IA	I	I
22	74	M	Lymphoma	HG NHL	Biopsy	IIIB	III	III (−)
23	67	M	Lymphoma	HD	Biopsy	IIB	II	II

*Metastasis was located in brain, which was not included in ^{18}F-FDG or ^{18}F-TYR study.

SCC = squamous cell carcinoma; LG = low grade; LCC = large cell carcinoma; HD = Hodgkin's disease; IG = intermediate grade; Adenoc. = adenocarcinoma; HG = high grade; (−) = fewer lesions were visualized; FN = false-negative.

Clinical stages obtained using conventional methods or after surgery are given according to American Joint Committee on Cancer.

uptake. Patients were injected intravenously with 2.8 ± 0.5 MBq/kg (0.07 ± 0.01 mCi/kg; mean ± SD) ^{18}F-FDG through an indwelling catheter. Acquisition was started 72 ± 17 min after injection and consisted of 5 or 6 bed positions. Five minute-emission scans, 1 min-transmission scans using a ^{137}Cs point source, and 8-s emission contamination scans were interleaved. On a separate day, patients received 2.2 ± 0.2 MBq/kg (0.06 ± 0.01 mCi/kg) ^{18}F-TYR through an indwelling catheter. Acquisition was started 36 ± 6 min after injections and followed the same procedure as for ^{18}F-FDG scanning. In addition, a second emission scan centered on a reference lesion was started after completion of the whole-body survey, 87 ± 9 min after injection. The time interval between the 2 acquisitions was thus 51 ± 7 min. Images were reconstructed using the ordered-subsets expectation maximization algorithm and corrected for decay, scatter, random events, and attenuation.

Data Analysis

For the purpose of this study, ^{18}F-FDG and ^{18}F-TYR PET scans were concurrently analyzed with full knowledge of all clinically relevant data. PET studies were first visually analyzed using the standard UGM software (UGM-Philips). Any focus visualized in the 3 planes that did not correspond to physiologic activity was considered as abnormal. Regions of interest (ROIs) were placed over these foci and followed an isocontour at 60% of the maximum pixel value. In addition, ROIs were placed over normal structures, including muscle (right deltoid), mediastinum, lungs, liver, bone marrow (body of a lower thoracic vertebra), and pancreas, only for ^{18}F-TYR. In all patients, these ROIs had similar sizes and were placed at similar levels. Standardized uptake values (SUVs) normalized for body weight (SUV_{bw}), for body surface area (SUV_{bsa}), and for lean body mass (SUV_{lbm}) were calculated using the following equations (*14*,*15*):

$$SUV_{bw} = \frac{\text{tissue concentration (MBq/mL)}}{\text{injected dose (MBq)/patient body weight (g)}}.$$

$$SUV_{bsa} = \frac{\text{tissue concentration (MBq/mL)}}{\text{injected dose (MBq)/BSA (m}^2\text{)}},$$

where BSA = 0.007184 × body weight$^{0.425}$ × body height$^{0.725}$.

$$SUV_{lbm} = \frac{\text{tissue concentration (MBq/mL)}}{\text{injected dose (MBq)/LBM}},$$

where LBM (women) = (1.07 × body weight) – 148 (body weight/body height)^2 and LBM (men) = (1.1 × body weight) – 120 (body weight/body height)^2.

Statistical Analysis

SUVs and activity ratios were compared in the different groups using 1-way ANOVA. Relationships between continuous variables were assessed using the Pearson product–moment correlation coefficient. In all cases, the level of significance was set at 0.05.

RESULTS

Whole-Body Distribution of ^{18}F-TYR

Uptake values in various organs, as well as their evolution over time and the corresponding SUVs obtained with ^{18}F-FDG, are shown in Figure 1. High uptake was seen in the pancreas and, to a lesser extent, in the liver and salivary glands. ^{18}F-TYR uptake was mild in the bone marrow, but significantly higher than ^{18}F-FDG. Muscle and liver uptakes were also higher with ^{18}F-TYR than with ^{18}F-FDG. Except for the SUV_{bw} measured in the bone marrow, ^{18}F-TYR uptake did not significantly increase over time.

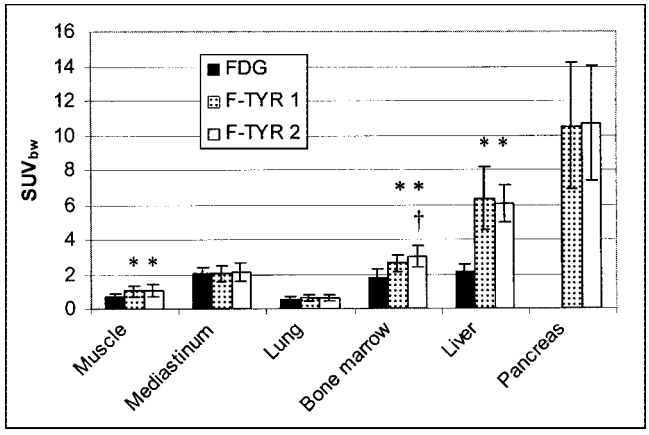

FIGURE 1. Uptake values in various organs (SUV_{bw}; mean ± 1 SD). F-TYR 1 = ^{18}F-TYR PET images taken at first time point; F-TYR 2 = ^{18}F-TYR PET images taken at second time point. *Statistically significant difference with ^{18}F-FDG. †Statistically significant difference between 2 ^{18}F-TYR time points. Because pancreas is normally not visualized on ^{18}F-FDG PET images, no regions were drawn. Except for bone marrow, where no difference was seen between ^{18}F-TYR 1 and ^{18}F-TYR 2, results obtained with SUV_{bsa} and SUV_{lbm} were similar to those obtained using SUV_{bw} and are not represented.

^{18}F-FDG Versus ^{18}F-TYR

^{18}F-FDG PET correctly identified 54 malignant lesions confirmed by pathologic analysis (n = 29) or correlative studies (n = 25). ^{18}F-TYR PET visualized 36 of 54 lesions (67%). Three additional lesions were seen only with ^{18}F-FDG: One mediastinal lymph node turned out to be benign (silicosis) on pathologic examination and the 2 other lesions, located in the lungs, remained unconfirmed. There was no false-positive result with ^{18}F-TYR. ^{18}F-FDG and ^{18}F-TYR scans provided similar results in terms of patients' staging in 6 of 11 lung cancers, in 2 of 2 head and neck carcinomas, and in 6 of 10 lymphomas, including 1 low-grade, stage I NHL that was missed by both modalities. One 11-mm large squamous cell carcinoma of the right upper lobe was not seen with ^{18}F-TYR PET (^{18}F-FDG SUV_{bw}, 2). One right lower lobe adenocarcinoma was visualized with ^{18}F-TYR PET (SUV_{bw}, 3.3) but not the extensive hilar and mediastinal involvement (^{18}F-FDG SUV_{bw}, ranging from 3 to 4.3). All nodal lesions were <1 cm on CT. Among 4 low-grade lymphomas, 1 was missed by both modalities, and 3 were similarly staged. There were 2 intermediate-grade NHLs. One patient had a large abdominal mass clearly seen with both ^{18}F-FDG and ^{18}F-TYR, but a biopsy-proven bone marrow involvement was equally missed. The other patient had stage III disease with matched results with both methods for all lymph node stations except the cervical, which was not visualized with ^{18}F-TYR. Two patients

had high-grade NHLs. In a stage IV disease, ^{18}F-TYR missed a massive splenic involvement and cervical nodes, whereas bilateral axillary nodes were clearly seen. In the second patient, bilateral cervical, abdominal, and right iliac nodes were missed by ^{18}F-TYR, which identified axillary, mediastinal, and left iliac nodes. There were 2 patients with Hodgkin's disease. One stage II was equally staged with both tracers. In a stage IV disease, ^{18}F-TYR was taken up by cervical and axillary nodes, but not by an extensive, biopsy-proven esophageal involvement or by a large vertebral spread confirmed by MRI.

Overall, SUVs were higher with ^{18}F-FDG than with ^{18}F-TYR. Both tumor-to-muscle and tumor-to-mediastinum activity ratios were also higher with ^{18}F-FDG than with ^{18}F-TYR. Detailed results are given in Table 1 and shown in Figures 2 and 3. Representative PET images are shown in Figures 4 and 5.

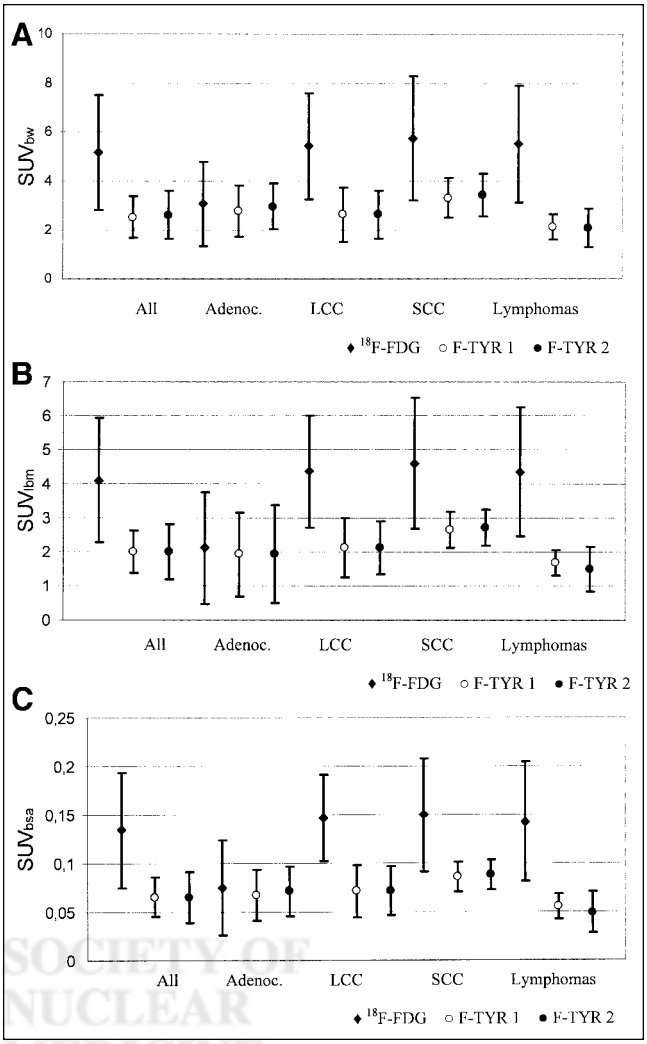

FIGURE 2. SUVs normalized for body weight (SUV_{bw}; A), lean body mass (SUV_{lbm}; B), and body surface area (SUV_{bsa}; C) in lesions that were seen with both tracers. Adenoc. = adenocarcinomas; LCC = large cell carcinomas; SCC = squamous cell carcinomas; F-TYR 1 = ^{18}F-TYR PET images taken at first time point; F-TYR 2 = ^{18}F-TYR PET images taken at second time point. Data are expressed as mean ± 1 SD.

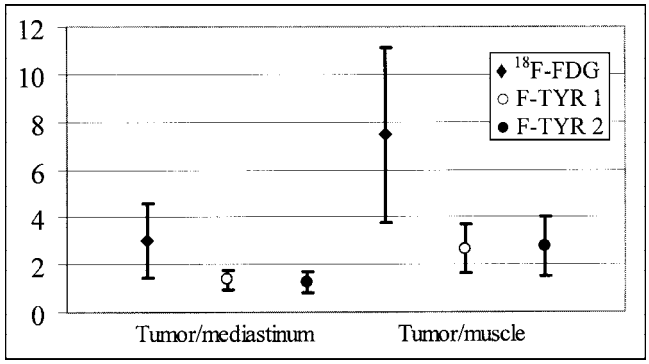

FIGURE 3. Activity ratios within tumors. Data are expressed as mean ± 1 SD.

Correlation Between ^{18}F-FDG and ^{18}F-TYR

There was a strong correlation between ^{18}F-FDG and ^{18}F-TYR uptake in the muscle, mediastinum, and lungs, regardless of the ^{18}F-TYR time point. A weak but signification correlation existed between ^{18}F-FDG and ^{18}F-TYR uptake measured at the initial time-point in the tumors. No correlation was found in the liver.

DISCUSSION

The nonspecific uptake of ^{18}F-FDG by inflammatory cells or granulation tissues is well known and has even led to widening its indications to various inflammatory or infectious diseases (*16*). However, this also limits its capability to accurately distinguish tumors from benign conditions, such as postradiation changes. Thus, a large number of other compounds—in particular, radiolabeled amino acids—has been investigated as an alternative or a complement to ^{18}F-FDG (*7,17*). Among these, ^{11}C-methyl-methionine

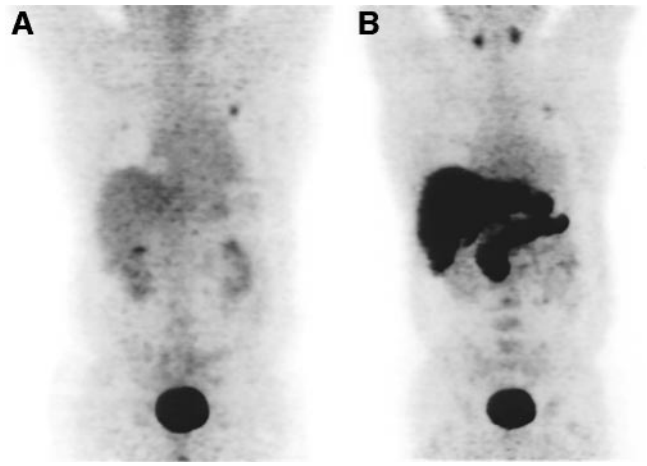

FIGURE 4. Three-dimensional projection PET images with ^{18}F-FDG (A) and ^{18}F-TYR (B) show 15-mm left upper lobe adenocarcinoma. ^{18}F-TYR uptake is high in pancreas, liver, and salivary glands and mild in bone marrow.

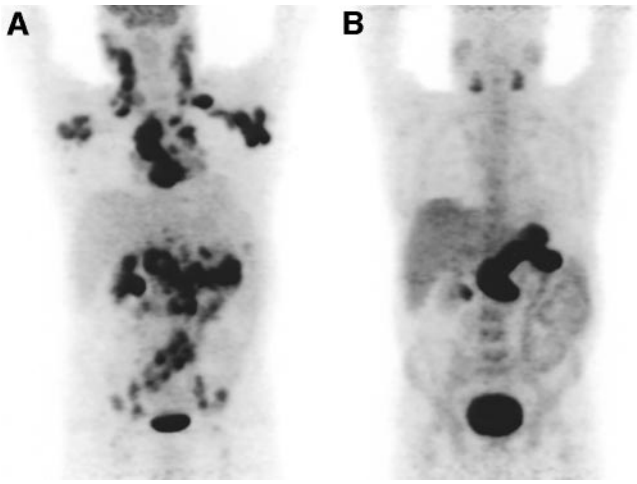

FIGURE 5. Three-dimensional projection PET images with ^{18}F-FDG (A) and ^{18}F-TYR (B) in patient with high-grade NHL. There is extensive nodal involvement on ^{18}F-FDG PET, whereas only mild uptake is seen in both axillary regions, upper mediastinum, and, using only centered 3-section viewing (not shown here), left iliac nodes with ^{18}F-TYR. Without extremely careful examination and without knowledge of ^{18}F-FDG results, ^{18}F-TYR scan could easily have been read as negative.

(MET) has been most extensively studied and has been shown to be valuable in brain tumors—in particular, for delineating the extent of the tumor (*18*). However, the tracer undergoes extensive nonprotein metabolism, with large amounts of circulating metabolites (*19*). The short half-life of ^{11}C also limits both the tracer availability and its whole-body imaging capability. Another ^{11}C-labeled compound that was extensively studied is L-1-^{11}C-tyrosine (^{11}C-TYR). Investigators at Groningen University obtained encouraging results with ^{11}C-TYR for evaluating primary brain tumors, breast, head and neck carcinomas, and sarcomas (*20–24*). It was not sensitive for detecting nonseminoma lesions (*25*). ^{11}C-TYR has established itself as a reliable tracer for assessing the rate of protein synthesis, but it shares with ^{11}C-MET the limitations of the short-lived isotope ^{11}C.

^{18}F-TYR was initially produced by Coenen et al. (*8*) using electrophilic radiofluorination of *O*-acetyltyrosine in CF_3CO_2H, with a radiochemical yield of 17% and a specific activity of 10–20 GBq/mmol. They first used a rodent model to demonstrate that the tracer is rapidly incorporated into proteins (>80% at 60 min after injection), with a small transfer RNA–bound fraction (1.5%–2%) and virtually no labeled metabolites. ^{18}F-TYR was thus featured as a tracer for evaluating the protein synthesis rate. Further studies in patients clearly showed that ^{18}F-TYR uptake was significantly higher in brain tumors than in the normal tissue, with better contrast obtained early on after injection because of the increase in plasma protein-bound ^{18}F-TYR over time (*9*). To date, however, there is no report of the use of ^{18}F-TYR for whole-body tumor imaging with PET.

We developed the synthesis of no–carrier-added ^{18}F-TYR by chiral catalytic phase-transfer alkylation, which improved both the radiochemical yield (25%–40%) and the specific activity (*10*). In patients, we found that most NSCLC and head and neck tumors were visualized as early as 30 min after injection. ^{18}F-TYR PET was less sensitive for detecting NHL and Hodgkin's disease lesions. However, overall, regardless of the normalization method (for body weight, body surface area, or lean body mass), the SUVs were higher with ^{18}F-FDG than with ^{18}F-TYR. On average, the SUVs and the tumor-to-mediastinum activity ratios were twice as high, and the tumor-to-muscle activity ratios were 3 times higher with ^{18}F-FDG than with ^{18}F-TYR. This was true for all tumor types except adenocarcinomas, where there was no significant difference (SUV_{bw}, 3.1 vs. 2.8 for ^{18}F-FDG and ^{18}F-TYR, respectively). It should be noted that only 3 lesions were seen with both modalities in this group, which greatly limits the significance of the average values. In the nonlymphoma tumors, all lesions missed with ^{18}F-TYR were small: There was one 11-mm primary adenocarcinoma and several metastatic nodes, also from an adenocarcinoma but in another patient. These nodes were also missed on CT. These false-negative results for ^{18}F-TYR can thus be attributed to the low tumor-to-background activity ratios observed with ^{18}F-TYR, which become critical in small lesions, rather than to a low protein synthesis rate or amino acid transport in these tumors. The average size of the lesions visualized with ^{18}F-TYR PET, as assessed by CT or pathologic examination, was 33 ± 17 mm in largest diameter.

In lymphoma patients, we observed a different pattern of results. Not only could ^{18}F-FDG–positive/F-TYR–positive lesions coexist with ^{18}F-FDG–positive/F-TYR–negative lesions in the same patient, but also the false-negative results with ^{18}F-TYR were not related to the lesions' size. This observation, quite unsettling, is clearly illustrated in Figure 5, which shows massive nodal involvement totally devoid of ^{18}F-TYR uptake, except in few regions. Although the series is limited and heterogeneous, no relationship was found between tumor grade or aggressiveness and tracer uptake. In these patients, we could not find any satisfactory explanation for the results obtained, which may be related to the heterogeneity that can arise among lymphomas and lead to clinical, biologic, or morphologic changes during the course of disease (composite lymphomas, lymphoma progression) (*26*). Differences in the local environment of the various tumor sites (angiogenesis, for instance) may also diversely influence the uptake of ^{18}F-TYR, whose mechanism in malignancies has yet to be fully understood. Experimental data are missing to sustain these hypotheses. To definitely answer this question would require obtaining pathologic samples from all lesions in all patients, which is obviously not possible.

The physiologic uptake of ^{18}F-TYR by normal structures can also limit the readability of the images and further decrease the sensitivity of the test. The high uptake in the pancreas and, to a lesser extent, the liver may limit the detection of lesions located in these organs. Similarly, the

significant uptake in salivary glands could hamper the staging of head and neck tumors, although de Boer et al. (*27*) recently reported 100% sensitivity with ^{11}C-TYR and PET for detecting primary carcinomas of the larynx and hypopharynx. On the other hand, we found that the ^{18}F-TYR uptake was fairly homogeneous in the soft tissue of the head and neck regions, which could constitute an advantage compared with ^{18}F-FDG, where intense uptake can be seen in lymphoid and muscular structures. Another concern is the significant uptake in the bone marrow, with an average SUV_{bw} of 2.6 ± 0.5 compared with 1.8 ± 0.5 with ^{18}F-FDG. Although Coenen et al. (*8*) found a significant amount of free ^{18}F-fluoride in the plasma at 40 min after injection, the uptake distribution observed in our patients clearly matched the normal bone marrow distribution. In particular, there was no uptake in long bones such as the humerus and femurs. There was only 1 case of bone marrow involvement in our population, and it was missed by both ^{18}F-FDG and ^{18}F-TYR PET studies. Because of the high physiologic uptake, ^{18}F-TYR is probably not the most appropriate tracer for evaluating pancreatic masses or for detecting bone or liver metastases.

There were no demonstrated false-positive results for ^{18}F-TYR in our series. Three lesions did take up ^{18}F-FDG but not ^{18}F-TYR and were considered false-positive: There were 2 lung lesions, unconfirmed by any other method, and 1 benign hilar lymph node, corresponding to silicosis on pathologic examination. The question of the specificity of radiolabeled amino acids remains unsettled. Initial studies reported low MET accumulation in inflammatory and granulation tissues (*6*,*28*,*29*). However, clinical studies using MET in lung cancer patients failed to improve the specificity over ^{18}F-FDG (*30*); recently, Rau et al. (*31*) found a higher MET uptake in inflamed lymph nodes than in tumor-infiltrated nodes in a murine model. These authors demonstrated that *O*-(2-^{18}F-fluoroethyl)-L-tyrosine (FET) did not accumulate into chronic and acute lymphadenitis models, with no overlap between tumor and inflammation uptake values (*31*). FET uptake by tumor cells depends on the L-transport system and it is not incorporated into proteins (*32*). Few data are available regarding the specificity of other amino acid analogs and, although our results are encouraging, no definite conclusion can be drawn.

In this study, the sensitivity for detecting various malignant lesions was relatively low, with only 67% of the lesions visualized with ^{18}F-FDG PET. This may be related to the biochemical processes studied with ^{18}F-TYR. Although initial studies showed a high and rapid incorporation of ^{18}F-TYR into newly formed proteins (*8*), further experiments from the same group using kinetic modeling indicated that an increase in the transport rate constant was primarily responsible for the high uptake in tumors (*9*). In the normal brain, the results fitted a 2-tissue compartment model (free intracellular ^{18}F-TYR and protein-bound ^{18}F-TYR). In tumors, however, a 3-tissue compartment model was better suited to explain the results. Ishiwata et al. (*33*) studied ^{18}F-TYR, L-methyl-^{3}H-MET, and L-1-^{14}C-leucine (^{11}C-LEU) in tumor-bearing mice. They found comparable protein incorporation for all 3 tracers, but the rate was much faster with ^{14}C-LEU. In another set of experiments, they showed that only ^{14}C-LEU uptake was decreased after inhibition of protein synthesis by cycloheximide, whereas the uptake of all 3 tracers was decreased after the amino acid transport was inhibited with ouabain (*34*). They also found significant amounts of radioactivity from ^{18}F-TYR in the lipid fraction of the tumor extracts. Along with the compartment modeling, these findings suggest, for ^{18}F-TYR, the presence of metabolic pathways distinct from the protein synthesis. These pathways remain unidentified. Therefore, in vivo, ^{18}F-TYR uptake is likely to represent both amino acid transport and protein synthesis, and possibly a third metabolic process, still unknown, in proportions that remain to be evaluated.

Furthermore, it has yet to be fully established whether protein synthesis or amino acid transport is the most appropriate phenomenon to evaluate for oncologic purposes. Although some studies showed a good correlation between transport, as measured by MET uptake, and the tumor-proliferating fraction (*35*,*36*), other work showed no correlation between tumor growth and transport (*37*). Amino acid metabolism is complex and non–protein synthesis pathways may also be significantly increased in tumor cells (*38*). Thus, tracers for transport may be as good as or even superior to synthesis tracers for in vivo imaging.

CONCLUSION

In our limited series, PET imaging with ^{18}F-TYR was less sensitive than ^{18}F-FDG for staging NSCLCs and lymphomas. Specificity may be improved with ^{18}F-TYR, but there were not enough false-positive results with ^{18}F-FDG to clearly establish any superiority. We thus believe that ^{18}F-TYR PET has, at best, a limited role for staging purposes, at least in these types of tumors.

ACKNOWLEDGMENTS

The authors express their appreciation to the staff of the PET center at the Centre Hospitalier Universitaire, Liège, and to the clinicians who participated to the recruitment of the patients. Part of this work was presented at the 49th Annual Meeting of the Society of Nuclear Medicine, Los Angeles, CA, June 15–19, 2002.

REFERENCES

1. Hustinx R, Benard F, Alavi A. Whole-body FDG-PET imaging in the management of patients with cancer. *Semin Nucl Med.* 2002;32:35–46.
2. Hofer C, Kubler H, Hartung R, Breul J, Avril N. Diagnosis and monitoring of urological tumors using positron emission tomography. *Eur Urol.* 2001;40:481–487.
3. Strauss LG. Fluorine-18 deoxyglucose and false-positive results: a major problem in the diagnostics of oncological patients. *Eur J Nucl Med.* 1996;23:1409–1415.
4. Isselbacher KJ. Sugar and amino acid transport by cells in culture: differences between normal and malignant cells. *N Engl J Med.* 1972;286:929–933.
5. Ishiwata K, Vaalburg W, Elsinga PH, Paans AM, Woldring MG. Comparison of

L-[1-^{11}C]methionine and L-[methyl-^{11}C]methionine for measuring in vivo protein synthesis rates with PET. *J Nucl Med.* 1988;29:1419–1427.
6. Kubota K, Matsuzawa T, Fujiwara T, et al. Differential diagnosis of AH109A tumor and inflammation by radioscintigraphy with L-[methyl-^{11}C]methionine. *Jpn J Cancer Res.* 1989;80:778–782.
7. Jager PL, Vaalburg W, Pruim J, de Vries EG, Langen KJ, Piers DA. Radiolabeled amino acids: basic aspects and clinical applications in oncology. *J Nucl Med.* 2001;42:432–445.
8. Coenen HH, Kling P, Stocklin G. Cerebral metabolism of L-[2-^{18}F]fluorotyrosine, a new PET tracer of protein synthesis. *J Nucl Med.* 1989;30:1367–1372.
9. Wienhard K, Herholz K, Coenen HH, et al. Increased amino acid transport into brain tumors measured by PET of L-(2-^{18}F)fluorotyrosine. *J Nucl Med.* 1991;32:1338–1346.
10. Lemaire C, Gillet S, Kameda M, et al. Enantioselective synthesis of 2-[^{18}F]fluoro-L-tyrosine by catalytic phase-transfer alkylation. *J Labelled Compds Radiopharm.* 2001;44:S857–S859.
11. Ooi T, Kameda M, Maruoka K. Molecular design of a C2-symmetric chiral phase transfer catalysis for practical asymmetric synthesis of α-amino acids. *J Am Chem Soc.* 1999;121:6519–6520.
12. Lemaire C, Damhaut P, Lauricella B, et al. Fast [^{18}F]FDG synthesis by alkaline hydrolysis on a low polarity solid phase support. *J Labelled Compds Radiopharm.* 2002;45:435–447.
13. Adam LE, Karp JS, Daube-Witherspoon ME, Smith RJ. Performance of a whole-body PET scanner using curve-plate NaI(Tl) detectors. *J Nucl Med.* 2001;42:1821–1830.
14. Sugawara Y, Zasadny KR, Neuhoff AW, Wahl RL. Reevaluation of the standardized uptake value for FDG: variations with body weight and methods for correction. *Radiology.* 1999;213:521–525.
15. DuBois D, DuBois EF. A formula to estimate the approximate surface area if height and weight be known. *Arch Intern Med.* 1916;17:863–871.
16. Zhuang H, Alavi A. 18-Fluorodeoxyglucose positron emission tomographic imaging in the detection and monitoring of infection and inflammation. *Semin Nucl Med.* 2002;32:47–59.
17. Laverman P, Boerman OC, Corstens FH, Oyen WJ. Fluorinated amino acids for tumour imaging with positron emission tomography. *Eur J Nucl Med Mol Imaging.* 2002;29:681–690.
18. Kaschten B, Stevenaert A, Sadzot B, et al. Preoperative evaluation of 54 gliomas by PET with fluorine-18-fluorodeoxyglucose and/or carbon-11-methionine. *J Nucl Med.* 1998;39:778–785.
19. Ishiwata K, Hatazawa J, Kubota K, et al. Metabolic fate of L-[methyl-^{11}C]methionine in human plasma. *Eur J Nucl Med.* 1989;15:665–669.
20. Kole AC, Plaat BE, Hoekstra HJ, Vaalburg W, Molenaar WM. FDG and L-[1-^{11}C]tyrosine imaging of soft-tissue tumors before and after therapy. *J Nucl Med.* 1999;40:381–386.
21. Kole AC, Pruim J, Nieweg OE, et al. PET with L-[1-carbon-11]tyrosine to visualize tumors and measure protein synthesis rates. *J Nucl Med.* 1997;38:191–195.
22. Plaat B, Kole A, Mastik M, Hoekstra H, Molenaar W, Vaalburg W. Protein synthesis rate measured with L-[1-^{11}C]tyrosine positron emission tomography correlates with mitotic activity and MIB-1 antibody-detected proliferation in human soft tissue sarcomas. *Eur J Nucl Med.* 1999;26:328–332.
23. Kole AC, Nieweg OE, Pruim J, et al. Standardized uptake value and quantification of metabolism for breast cancer imaging with FDG and L-[1-^{11}C]tyrosine PET. *J Nucl Med.* 1997;38:692–696.
24. Pruim J, Willemsen AT, Molenaar WM, et al. Brain tumors: L-[1-C-11]tyrosine PET for visualization and quantification of protein synthesis rate. *Radiology.* 1995;197:221–226.
25. Kole AC, Hoekstra HJ, Sleijfer DT, Nieweg OE, Schraffordt Koops H, Vaalburg W. L-[1-carbon-11]tyrosine imaging of metastatic testicular nonseminoma germ-cell tumors. *J Nucl Med.* 1998;39:1027–1029.
26. Müller-Hermelink HK, Zettl A, Pfeifer W, Ott G. Pathology of lymphoma progression. *Histopathology.* 2001;38:285–306.
27. de Boer JR, van der Laan BFM, Pruim J, et al. Carbon-11 tyrosine PET for visualization and protein synthesis rate assessment of laryngeal and hypopharyngeal carcinomas. *Eur J Nucl Med Mol Imaging.* 2002;29:1182–1187.
28. Kubota R, Kubota K, Yamada S, et al. Methionine uptake by tumor tissue: a microautoradiographic comparison with FDG. *J Nucl Med.* 1995;36:484–492.
29. Kubota K, Kubota R, Yamada S, Tada M. Effects of radiotherapy on the cellular uptake of carbon-14 labeled L-methionine in tumor tissue. *Nucl Med Biol.* 1995;22:193–198.
30. Nettelbladt OS, Sundin AE, Valind SO, et al. Combined fluorine-18-FDG and carbon-11-methionine PET for diagnosis of tumors in lung and mediastinum. *J Nucl Med.* 1998;39:640–647.
31. Rau FC, Weber WA, Wester HJ, et al. *O*-(2-[^{18}F]fluoroethyl)-L-tyrosine (FET): a tracer for differentiation of tumour from inflammation in murine lymph nodes. *Eur J Nucl Med Mol Imaging.* 2002;29:1039–1046.
32. Heiss P, Mayer S, Herz M, Wester HJ, Schwaiger M, Senekowitsch-Schmidtke R. Investigation of transport mechanism and uptake kinetics of O-(2-[^{18}F]fluoroethyl)-L-tyrosine in vitro and in vivo. *J Nucl Med.* 1999;40:1367–1373.
33. Ishiwata K, Kubota K, Murakami M, Kubota R, Senda M. A comparative study on protein incorporation of L-[methyl-^{3}H]methionine, L-[1-^{14}C]leucine and L-2-[^{18}F]fluorotyrosine in tumor bearing mice. *Nucl Med Biol.* 1993;20:895–899.
34. Ishiwata K, Kubota K, Murakami M, et al. Re-evaluation of amino acid PET studies: can the protein synthesis rates in brain and tumor tissues be measured in vivo? *J Nucl Med.* 1993;34:1936–1943.
35. Leskinen-Kallio S, Nagren K, Lehikoinen P, Ruotsalainen U, Joensuu H. Uptake of ^{11}C-methionine in breast cancer studied by PET: an association with the size of S-phase fraction. *Br J Cancer.* 1991;64:1121–1124.
36. Miyazawa H, Arai T, Iio M, Hara T. PET imaging of non-small-cell lung carcinoma with carbon-11-methionine: relationship between radioactivity uptake and flow-cytometric parameters. *J Nucl Med.* 1993;34:1886–1891.
37. Bading JR, Kan-Mitchell J, Conti PS. System A amino acid transport in cultured human tumor cells: implications for tumor imaging with PET. *Nucl Med Biol.* 1996;23:779–786.
38. Ishiwata K, Enomoto K, Sasaki T, et al. A feasibility study on L-[1-carbon-11]tyrosine and L-[methyl-carbon-11]methionine to assess liver protein synthesis by PET. *J Nucl Med.* 1996;37:279–285.